Micropipette Suction for Measuring Piconewton Forces of Adhesion and Tether Formation from Neutrophil Membranes

Jin-Yu Shao and Robert M. Hochmuth
Department of Mechanical Engineering and Materials Science, Duke University, Durham, North Carolina 27708-0300 USA

ABSTRACT A new method for measuring piconewton-scale forces that employs micropipette suction is presented here. Spherical cells or beads are used directly as force transducers, and forces as small as 10–20 pN can be imposed. When the transducer is stationary in the pipette, the force is simply the product of the suction pressure and the cross-sectional area of the pipette minus a small correction for the narrow gap that exists between the transducer and the pipette wall. When the transducer is moving along the pipette, the force on it is corrected by a factor that is proportional to the ratio of its velocity relative to its drag-free velocity. With this technique, the minimum force required to form a membrane tether from neutrophils is determined (45 pN), and the length of the microvilli on the surface of neutrophils is inferred. The strength of this technique is in its simplicity and its ability to measure forces between cells without requiring a separate theory or a calibration against an external standard and without requiring the use of a solid surface.

INTRODUCTION

Specific adhesion between a cell and another cell or a solid surface occurs because bonds are formed between membrane receptors and their ligands. Once having adhered, cells can detach by several postulated mechanisms, including 1) the dissociation or breaking of the molecular bond or bonds, 2) the separation or extraction of receptors from the membrane, and 3) the failure of the membrane in which the receptors are embedded. Regardless of the process, measurement of the force of separation is fundamental to our understanding of the biological processes of adhesion and detachment. Thus, the purpose of this paper is to establish a simple method, based on micropipette suction, that allows the accurate measurement of the force of detachment of one cell from another cell or a solid surface. The limitation of the method, as presented here, is that one of the cells must fit snugly in a pipette and act as a frictionless piston that transduces a suction pressure into a force. Another limitation is that forces smaller than approximately 10–20 pN cannot be measured accurately when the pipette diameter is as large as 10 μm. The strength of the method is in its simplicity and its ability to measure forces between cells without requiring a separate theory or a calibration against an external standard and without requiring the use of a solid surface, such as a plastic bead, or a specialized surface, such as a smooth-walled capsule.

Several ingenious methods have been developed for measuring small forces between cells and surfaces. In general, the methods involve the precise measurement of a deflection by use of optical microscopy and, in some cases, interferometry. The deflection is transduced into a force by, for example, the cantilever beam in an atomic force microscope (Binnig et al., 1986; Hoh et al., 1992; Florin et al., 1994; Moy et al., 1994; Dammer et al., 1995), a microneedle (Kamimura and Takahashi, 1981; Kishino and Yanagida, 1988; Ishijima et al., 1991; Kojima et al., 1994), a laser photon trap, or "tweezers" (Ashkin, 1992; Kuo and Sheetz, 1992, 1993; Finer et al., 1994), and a smooth-walled membrane capsule inflated by micropipette suction (Evans et al., 1991, 1995). Calibration of the force-deflection relation comes from dragging a beam (as in the case of the atomic force microscope) or a microneedle or a bead (as in the case of the laser tweezers) through water at low Reynolds number and using appropriate hydrodynamic formulas that predict the fluid drag force as a function of velocity and size. For the inflated membrane capsule, calibration comes directly from the theory describing the deflection of the smooth membrane surface. To our knowledge, all these measurements require the use of specialized surfaces, such as a plastic bead in a laser trap, a metal tip on the end of a cantilever beam, or a smooth-walled membrane surface.

Another method for deducing the force of detachment involves the arrest of rolling cells on surfaces in a parallel-plate flow channel (Alon et al., 1995). Here the force is calculated from the hydrodynamic equations that predict the force and torque on a sphere adhering to a surface and from an assumption of the length of the moment arm between the point of rolling and the point of attachment.

In the method presented here a freely sliding spherical cell, in this case a human neutrophil, in a micropipette is allowed to adhere to a plastic bead coated with antibodies to particular adhesion receptors. (The bead is used here for the sake of convenience. It can be replaced by another cell or by any other surface.) Then the force F on the static cell is simply the suction pressure Δp, as determined from the hydrostatic head of a water-filled reservoir, times the cross-sectional area of the pipette:

$$F = \pi R_p^2 \Delta p, \quad (1)$$

Received for publication 29 May 1996 and in final form 23 August 1996.
Address reprint requests to Dr. Robert M. Hochmuth, Department of Mechanical Engineering and Materials Science, Duke University, Durham, NC 27708-0300. Tel.: 919-660-5310; Fax: 919-660-8963; E-mail: hochmuth@acpub.duke.edu.

0006-3495/96/11/2892/10 $2.00

where R_p is the radius of the pipette. The freely sliding cell is the force transducer. No calibration is required for a static cell because hydrostatic pressure is a primary standard. In the course of the study it was discovered that, when the force on the neutrophil exceeded a critical value of ~45 pN, the cell no longer remained static but formed a membrane tether that allowed it to move away from the bead at a constant velocity until it detached. In this case the force on the cell is diminished and must be calculated by use of a modification, given below, to Eq. 1.

MATERIALS AND METHODS

Neutrophil preparation

Two neutrophil preparation procedures were employed that correspond to two different ways of obtaining blood: venipuncture and finger prick.

Venipuncture

The exact procedures for isolating neutrophils from venous blood in a sterile environment were described in the literature (Needham et al., 1989). Briefly, the human peripheral blood of a healthy donor was drawn into a K_2EDTA vacutainer and was centrifuged at 300 g for 25 min at room temperature (~20°C). Some of the plasma was filtrated with 0.2-μm filters into cryogenic vials, which were then sealed tightly with caps, covered with parafilm, and stored in a freezer for future use as the medium for finger prick blood. The rest of the plasma and the buffy coat were diluted to 50% (v/v) with modified endotoxin-free Hanks balanced salt solution (HBSS; Sigma, St. Louis, MO; no Ca^{2+} or Mg^{2+}), which was buffered with 25 mM Hepes. The diluted solution was centrifuged over Ficoll-Hypaque gradients (Sigma, St. Louis, MO) at 700 g for 20 min at room temperature (~20°C). The cells at the 1077/1119 interface were collected and washed twice with HBSS. Finally, the cells were resuspended in 50% autologous plasma/HBSS.

Finger prick

The stored plasma as described in the previous paragraph was taken out of the freezer and warmed to room temperature (~20°C); then the plasma was diluted to 50% by addition of the same volume of HBSS. The blood was obtained by finger prick and was collected into a heparinized capillary glass tube (1.5 mm × 1.1 mm × 75 mm; Clay Adams, Parsippany, NJ). The blood end of the tube was sealed with Critoseal tube sealant, and the tube was centrifuged at 13,450 g for 1 min at room temperature (~20°C). Thereafter, near the plasma–erythrocyte interface, the tube was cut at a point on the side of the erythrocytes. The erythrocytes were thrown away, and the plasma and the rest of the cells were resuspended in a 0.1-ml 50% autologous plasma–HBSS solution. The solution was centrifuged at 2700 g for 2 min at room temperature (~20°C). Finally, the top layer at the plasma–erythrocyte interface was collected and added to the experimental chamber.

Bead preparation

The latex beads coated with goat antimouse IgG (specific to the Fc portion of mouse IgG) were purchased from Sigma (St. Louis, MO). Two drops of uniformly mixed beads (~0.1 ml) were put into an Eppendorf tube and washed with phosphate-buffered saline (PBS; containing 121.5 mM NaCl, 25.2 mM Na_2HPO_4, and 4.8 mM KH_2PO_4; pH 7.4, 300 mOsm) twice. The beads were resuspended in 0.3-ml PBS, to which 10 μl of monoclonal mouse antihuman antibodies were also added. This antibody–bead mixture was incubated at 37°C for 1 h, during which the mixture was shaken every 20 min. Finally, the beads were washed with PBS once and resuspended in PBS. Three antibodies were used in the experiment: anti-CD18 and anti-CD62L (Becton-Dickinson, San Jose, CA) as well as anti-CD45 (Sigma, St. Louis, MO).

Micropipette preparation

A glass tube (0.75 mm × 0.4 mm × 15.2 mm; A-M Systems, Inc., Everett, WA) was heated at the center and pulled apart with a vertical pipette puller (Model 700C; David Kopf Instruments, Tujunga, CA). Thus, two microneedles with a cylindrical, hollow inside were formed. Different heating rates and pulling forces could give different shapes of microneedles. One of the microneedles was cut at a desired position by a microforge to create a micropipette with a smooth opening. The first 10 mm of the micropipette was filled with 50% plasma (diluted from pure plasma by addition of HBSS) at the beginning of an experiment, and the rest of it was backfilled with PBS.

Micropipette manipulation and pressurization

Since the pioneering work of Mitchison and Swann (1954) and Rand and Burton (1964), micropipette manipulation has developed into a sophisticated technique for studying the properties of erythrocytes (Evans, 1973; Hochmuth et al., 1983) and leukocytes (Evans and Kukan, 1984). As shown in Fig. 1, a micropipette is inserted into an experimental chamber, which we made by covering a gap formed between two parallel microslides with cover slips. The other end of the micropipette is connected to Tygon tubing through a micromanipulator, which can move the micropipette in three dimensions. The tubing goes to a reservoir, which is open to air, and the whole pathway is filled with water. The reservoir can be moved up or down with a micrometer that has a resolution of 2.5 μm, which corresponds to a pressure change of 0.25 dyn/cm^2, or 0.025 pN/μm^2 (1 pN/μm^2 = 1 N/m^2). One can also change the pressure by blowing or sucking air into or out of the reservoir. In fact, because of the evaporation of the fluid in the chamber, the pressure could change during an experiment. Consequently, a chamber with only a small area exposed to air (25 mm × 6 mm × 2 mm) was used to minimize evaporation, and we frequently checked the zero-pressure setting for the micrometer during an experiment by finding the point where there was no flow in the pipette as observable by the presence of small particles or cells in suspension. Another micropipette manipulation system can be set up on the other side of the chamber to hold another cell or bead. Fig. 2 shows an example of simultaneous manipulation with two micropipettes.

Video analysis

Time was measured field by field (the time difference between two adjacent fields is 0.017 s). Distance was measured with video calipers

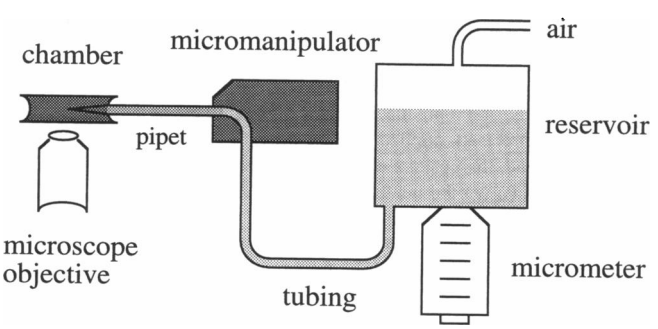

FIGURE 1 Schematic representation of the micropipette manipulation system.

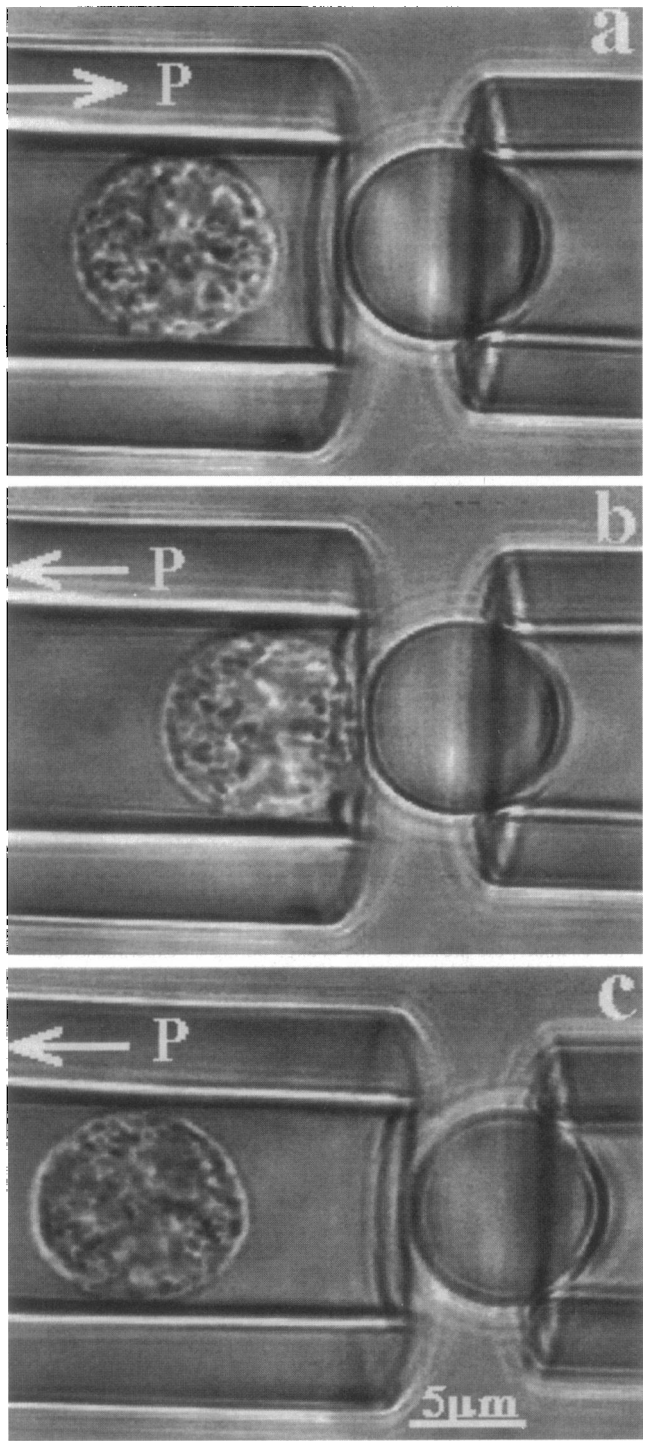

FIGURE 2 Cell adhesion and detachment: (*a*) the neutrophil is brought to the tip of the micropipette by application of a positive pressure that overcomes a precisely applied suction pressure; (*b*) after the neutrophil touches the bead, the positive pressure is released, and the precise suction pressure remains; (*c*) the neutrophil moves away freely from the bead if there is no adhesion between cell and bead. It should be noted that, if adhesion occurs, the neutrophil will either remain in contact with the bead for a while or move away at a smaller velocity, as though on a tether.

(Model 305, Vista Electronics, La Mesa, CA) that we calibrated before every experiment by using a recorded image of a micrometer.

Cell contact and adhesion

As shown in Fig. 2, a bead was partially aspirated by a micropipette (the bead pipette) whose diameter was smaller than the diameter of the bead, so the bead stayed fixed at the tip of this pipette. A neutrophil was aspirated into another micropipette (the neutrophil pipette) whose diameter was slightly smaller than or equal to the diameter of the neutrophil, so the neutrophil sealed the pipette and yet moved freely in it. The bead was positioned at the opening of the neutrophil pipette, and the height of the reservoir was adjusted until the neutrophil stayed stationary (the zero-pressure state). We applied a precise suction pressure by turning the micrometer, and this caused the neutrophil to move in the direction of the reservoir (Fig. 1). Then we applied a positive pressure by gently expelling air (using lung pressure) into the reservoir so the neutrophil was brought back to the tip of the pipette (Fig. 2 *a*). When the neutrophil and the bead made contact, the positive pressure was released, leaving only the previously applied suction pressure (Fig. 2 *b*). If the neutrophil and the bead adhered to each other, the cell remained static. Otherwise, the neutrophil would move away from the bead (Fig. 2 *c*). The whole process was recorded on a video tape at a speed of 60 fields/s.

RESULTS

Apparent film thickness

No adhesion between cell and pipette wall was observed in these experiments, as we verified by plotting cell velocity versus suction pressure and showing that the linear relationship extrapolated to zero (Fig. 3) and showing that a cell in the pipette moved readily when the smallest detectable suction pressure (~0.025 pN/μm^2) was applied to it. The cell moves as though surrounded by a thin film of water. The "apparent" thickness of this film can be calculated from the analysis given in the appendixes, where the cell is modeled as a smooth-walled concentric sphere in a tube. From a measurement of the equivalent length of the micropipette (Appendix A) and measurements such as those shown in Fig. 3, a value for the apparent film thickness can be calculated as shown in Appendix C. A typical value in

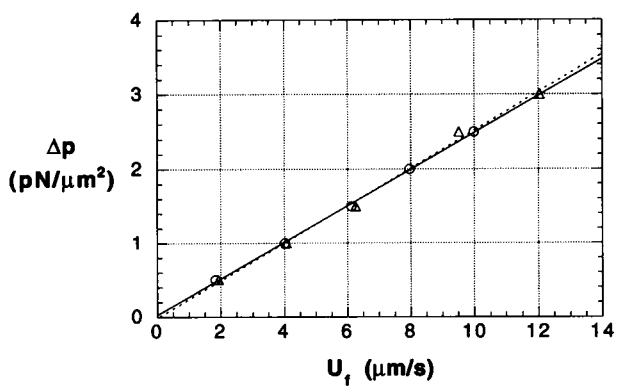

FIGURE 3 The "free" velocity (U_f) of two neutrophils, represented by either ○ or △, at different suction pressures (Δp) in a 9.5-μm micropipette. The extrapolation to zero velocity of the fitted lines lies within the pressure resolution of the system.

these experiments is 0.1 μm. This small value for the apparent gap width means that the force on a static, adherent cell can be calculated by Eq. 1 because the higher-order correction terms, as shown in Eq. B22 and Appendix D, can be neglected.

Length of a microvillus

The distal edge of a neutrophil (Fig. 2) is "tracked" as the cell approaches the bead, touches it, and then either adheres or immediately moves away from the bead under the action of the suction pressure. Fig. 4a compares the motion of the cell for these two cases. (The zero location on the ordinate is given by the point where the cell touches the bead.) The force of 35 pN exerted on the adherent, static cell (open circles) is calculated from Eq. 1. Note that the adherent cell in Fig. 4 *a* rebounds slightly to a point that is ~0.2 μm from the point of contact. This distance probably is a measure of the length of a microvillus plus the length of the antigen–antibody molecular bond because the bead is coated with an antibody to L-selectin and L-selectin is known to be concentrated at the tips of the microvilli of passive neutrophils (Picker et al., 1991; Erlandsen et al., 1993). This average rebound distance for six neutrophils touching L-selectin antibody-coated beads is 0.62 μm for cell forces of ~35 pN.

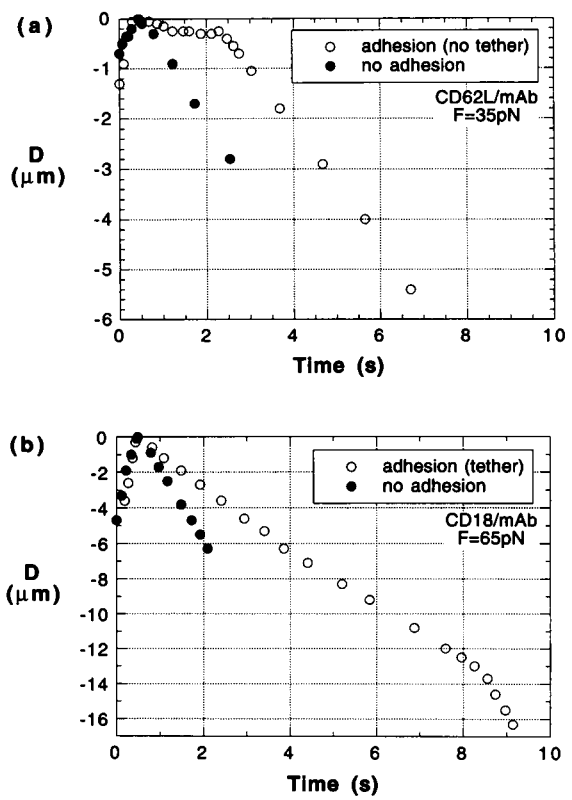

FIGURE 4 Tracking the distal edge of the neutrophil as it touches a bead, where D is the distance from the point of zero velocity: ●, curves where no adhesion occurs; ○, cases where adhesion occurs and the cell either (*a*) remains static or (*b*) moves away from the bead on a membrane tether.

Formation of tethers

When the calculated force on a cell (Eq. 1) exceeds a value of ~45 pN, an adherent cell no longer remains static but moves downstream at a constant velocity that is significantly less than the velocity of a nonadherent cell. Such a cell is shown by the open circles in Fig. 4 *b*. Note that this slower-moving cell eventually pulls free after ~8 s and quickly accelerates to a velocity that matches that of the nonadherent cell, shown by the filled circles in Fig. 4 *b*. This retarded motion is caused by a membrane tether that is extracted from the surface of the neutrophil and that connects the cell to the bead even as the cell moves downstream at a constant velocity. In these experiments the tether is not seen until it pulls free from the bead. When this occurs there is no net force on the tether (and the cell), and this allows the tether to expand rapidly in diameter until it can be observed as a faint shadow.

The net force on a static cell is given by Eq. 1, and the net force on a freely moving cell is zero. (This "drag-free" condition for a freely moving cell means that the net pressure force acting over the surface of the cell in the direction of motion is exactly balanced by the net fluid shear force acting over the surface of the cell in the same direction.) Thus, the force on a tethered cell will have some value between zero and that given by Eq. 1. An analysis given in Appendix B of the motion of a concentric sphere in a tube shows that the force on a tethered cell can be calculated from the simple equation (Eq. D3) in Appendix D:

$$F = \Delta p \pi R_p^2 \left(1 - \frac{U_t}{U_f}\right), \tag{2}$$

where U_t is the velocity of the tethered cell and U_f is the velocity of the freely moving cell. The general form of Eq. 2 is apparent. When $U_t = 0$ (i.e., an adherent cell with no tether), Eq. 1 is obtained, and when $U_t = U_f$ (i.e., the tether detaches from the bead and the cell moves freely), the force on the cell is zero. The force of 65 pN exerted on the tethered cell shown in Fig. 4 *b* is calculated from Eq. 2. The neutrophil acts as its own control when Eq. 2 is used to calculate the force. That is, U_t is measured from the slope of the line for the tethered cell in Fig. 4 *b* and U_f is measured from the slope of the same line after the tether has detached from the bead. In Fig. 4 *b* this occurs after the 8-s mark.

The velocity of a tethered neutrophil versus the force (calculated from Eq. 2) exerted on the cell is shown in Fig. 5 for cells tethered to beads coated with antibodies to L-selectin (CD62L), the β_2 integrins (CD18), and the membrane glycoprotein CD45. Each point in this figure represents the average tether velocity for at least 9 and at most 12 cells. The results appear to be independent of the antibody used to coat the bead and show, from a linear extrapolation, that the minimum force required for formation of a neutrophil membrane tether is 45 pN. The force on a tethered cell increases linearly with an increase in velocity. Similar behavior has been observed for tethers pulled from red cells

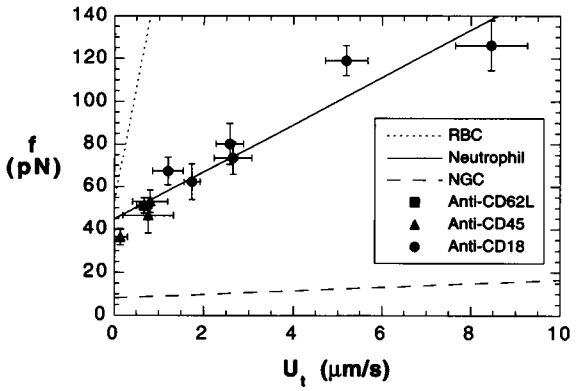

FIGURE 5 Linear correlation between the tether growth velocity (U_t) and the force applied on the tether (f). Error bars in both directions stand for the respective standard deviations in the experimental measurement. Also shown are the results for tethers extracted from red blood cells (*RBC*, Waugh and Bauserman, 1995) and neuronal growth cones (*NGC*, Dai and Sheetz, 1995; Hochmuth et al., 1996).

(Waugh and Bauserman, 1995) and neuronal growth cones (Dai and Sheetz, 1995; Hochmuth et al., 1996).

DISCUSSION

The results show that it is a simple matter to determine the force of adhesion between a cell and another cell or foreign surface, as long as the cell does not adhere to the pipette wall. The results show also that the adhesion "lifetime" can be measured. For example, Fig. 4 *a* indicates that the lifetime of the adhesive bond persists for ~2 s, although it is interesting to note that some small motion is observed before detachment occurs. Perhaps this is due to the extension of a previously flattened microvillus that has adhered at its tip to the bead when contact occurred between cell and bead. Fig. 4 *b* shows a much longer lifetime even though the force is larger and, as a consequence, a membrane tether had been extracted from the cell. However, a different molecular bond is being formed in this case because a different antibody is being used to coat the bead. The adhesive bond in Fig. 4 *b* withstands a larger force and persists for a longer time than the one formed in Fig. 4 *a*. In all cases, it is likely that these are forces between single molecular bonds because adhesion between cell and bead occurs only rarely (<20%) when the cell touches the bead.

Membrane tethers are "instantaneously" formed when the adhesive force exceeds a critical value of ~45 pN. It may be that such membrane tethers form when cells roll on selectin-coated surfaces and, thus, tethers may play a fundamental role in this interesting and important phenomenon. For example, the recent research of Alon et al. (1995) shows that neutrophils in a fluid shear flow produced in a parallel-plate flow channel roll on surfaces coated with P-selectin. Alon et al. show that single bonds can be formed between P-selectin and its counterreceptor on the neutrophil. Furthermore, they postulate that the length of the moment arm between the point of rigid-body rotation and the point of molecular attachment is 4 μm and that the cell has a radius of 4.25 μm. Thus, for a particular shear stress of 1.1 dyn/cm^2 in their experiments and for this particular moment arm, they calculate a force at the point of molecular attachment of 112 pN and a bond angle from the horizontal of 55.5°. Furthermore, at this force they measure a bond lifetime of ~0.29 s. According to the data presented in Fig. 4, the tether growth rate at a force of 112 pN is ~6 μm/s, so in 0.3 s a tether will grow to a length of 1.7 μm. This distance is almost exactly the length required for connection of a spherical cell to a flat surface when the angle of attachment is 55.5° and the moment arm from the point of rolling to the point of tether formation is 4 μm. Note that a microvillus alone (Fig. 4 *a*) is not long enough to traverse this distance, but a membrane tether is because of its rapid growth for forces in excess of ~45 pN.

It is possible to estimate the radius of the tether by using a formula first derived by Waugh and Hochmuth (1987):

$$f_0 = 2\pi B/R_t, \tag{3}$$

where B is the bending modulus of the membrane forming the tether, R_t is the tether radius, and f_0 is the tether force at zero velocity (45 pN). If it is assumed that $B = 3 \times 10^{-19}$ J = 0.3 pN · μm (a value typical of that for phospholipid bilayers, red cell membranes, and neuronal growth cone membranes), then the estimated value for the tether radius is $R_t = 2\pi \times 0.3$ pN · μm/45 pN = 0.04 μm = 40 nm. It is possible also to calculate the "apparent surface tension" for the neutrophil membrane from the research of Hochmuth et al. (1996):

$$f_0 = 2\pi\sqrt{2B(T + \gamma)}, \tag{4}$$

where T is the "far-field" tension in the membrane and γ is the energy of adhesion between membrane and cytoskeleton. (In the derivation of Eq. 4, the energy of adhesion represented by γ was assumed to be reversible. This may not be the case when tethers are extracted from neutrophils, so the calculation with Eq. 4 can be considered only an estimate.) Again using an assumed value for B of 0.3 pN · μm gives a value for $(T + \gamma)$ of 85 pN/μm. Now, the cortical tension T has been measured in separate experiments using micropipette aspiration and the law of Laplace (Evans and Yeung, 1989; Needham and Hochmuth, 1992) and has a value of ~30 pN/μm. If it is assumed that the cortical tension and the far-field tension are the same, then the energy of adhesion between neutrophil membrane and its cytoskeleton, γ, should have a value of ~55 pN/μm = 55×10^{-6} J/m^2 = 5.5×10^{-17} J/μm^2.

It is seen from the results in Fig. 4 that neutrophils detach from surfaces after a certain lifetime and that neutrophils can even form membrane tethers before they detach. It is unlikely that detachment occurs because of membrane failure because the membrane tensions in these experiments, ~80 pN/μm, are 2 orders of magnitude less than the isotropic tensions of ~10^4 pN/μm that cause membrane failure. This would leave two mechanisms for detachment:

either a molecular receptor–ligand bond fails or the receptor is extracted from the membrane. The former mechanism is favored by the study of Alon et al. (1995) and is usually the postulated mechanism in models of cell detachment (Dembo et al., 1988). Detachment occurs by the latter mechanism when agglutinin-bounded red cells are separated (Evans et al., 1991). Perhaps both mechanisms are at work when neutrophils detach, with receptor extraction being the dominant mechanism of failure when tethers are formed. In this case, the adhesion receptors may be separated from the cytoskeleton because the cytoskeleton is likely to be considerably thicker than the diameter of the tether (Zhelev et al., 1994) and, thus, would not fit into the tether but would remain behind at the surface of the cell body. Without the cytoskeleton, receptors would be less firmly anchored in the lipid bilayer membrane and might be more easily extracted. Determining which mode of detachment is the dominant one and characterizing the force-lifetime behavior of the two different modes and the possible interplay between them, especially for the case when tethers are formed, remains a challange for future studies.

This research was supported by National Institutes of Health Grant RO1-HL23728. We would like to thank Dr. Doncho Zhelev for helpful discussions about these experiments. Our thanks also extend to the help of Clinical Research Unit of Duke University Medical Center, which is supported by MO1-RR-30 of the GCRC program.

APPENDIX A. EQUIVALENT LENGTH OF THE MICROPIPETTE, L_{eq}

Although the diameter of the micropipette is constant near the tip, the fact that the diameter increases along the axis cannot be ignored when fluid flow inside the micropipette is considered. If the diameter changes slowly (which is the case here), the flow can still be characterized as Poiseuille flow (Happel and Brenner, 1983). However, the real length of the micropipette cannot be directly used in the Poiseuille formula. Instead, an equivalent length, L_{eq}, is defined as

$$L_{eq} \equiv \frac{\pi D_p^4 \Delta p}{128 \mu Q}, \tag{A1}$$

where Δp is the pressure drop from the tip of the micropipette to the reservoir, D_p is the diameter at the opening of the micropipette, μ is the viscosity of the fluid, and Q is the volumetric flow rate when no cells are present. In other words, the pressure–flow relationship in the micropipette is equivalent to that in a uniform tube with diameter D_p and length L_{eq}.

Zhelev and Needham (1993) obtained a value of 922 μm for the equivalent length of their micropipette by measuring the velocities of small latex beads and liposomes under different suction pressures. Here, we measured L_{eq} by positioning the micropipette when it was free of cells at a cell-free area of the chamber, applying a suction pressure to the pipette, and observing the motion of small particles (platelets or granules) less than 1 μm in diameter. Inasmuch as the diameter of the pipette was ~9.5 μm, it was assumed that these small particles have the same velocity as the surrounding fluid (Happel and Brenner, 1983). Only the velocities of particles moving at the center line of the pipette were measured. In fact, it was difficult to detect whether a particle was precisely at the center, so all the velocities of the particles that were close to the center were measured, and the maximum velocity obtained was used to estimate the center-line velocity (Fig. 6). The pressure range used here represented the pressure

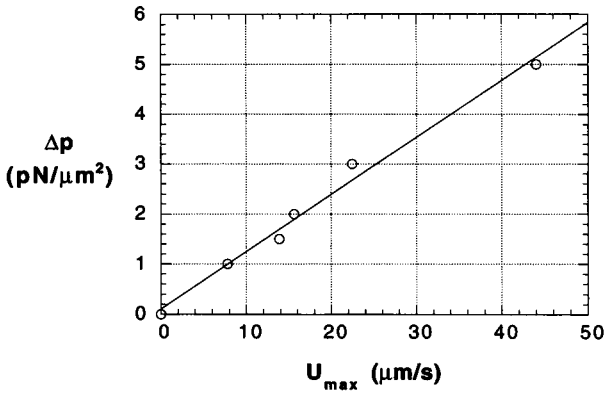

FIGURE 6 Velocities (U_{max}) of small particles moving at or near the center line of the pipette at different suction pressures (Δp). The slope of this line is 0.114 pN · s/μm^3.

range used in the tether-formation experiments. With $Q = \pi D_p^2 U_{max}/8$, the equivalent length is calculated from Fig. 6 and Eq. A1:

$$\begin{aligned} L_{eq} &= \left(\frac{\Delta p}{U_{max}}\right)\frac{D_p^2}{16\mu} \\ &= 0.114 \frac{\text{pN } s^{-1}}{\mu\text{m}^3} \frac{(9.5)^2 \mu\text{m}^2}{16 \times 0.001 \text{ pN} \cdot \text{s}/\mu\text{m}^2} \\ &\approx 650 \ \mu\text{m}. \end{aligned} \tag{A2}$$

The shapes of micropipettes made when the same heating rate and pulling force are used are very consistent (unpublished data), so it is reasonable to assume that the micropipettes used here have the same equivalent length.

APPENDIX B. MOTION OF A TETHERED OR FREELY MOVING SPHERE IN A UNIFORM CIRCULAR TUBE

Here, a neutrophil is modeled as a smooth-walled sphere moving at low Reynolds number, and a lubrication theory analysis is performed. As shown in Fig. 7 *a*, a sphere is centered in a circular, fluid-filled tube and moves along the axis of the tube at a velocity U. If a force F is applied in the opposite direction of U, then the sphere will move at a smaller constant velocity. In other words, the sphere will have a retarded motion. For a given average fluid velocity, U and F are correlated, i.e., for any given F there is only one corresponding constant velocity U. Obviously, when $F = 0$ the sphere is "drag free," and when F reaches a maximum value $U = 0$, which corresponds to a stationary sphere. Assume that the pressure drop over the whole tube is Δp. Δp consists of two parts: the pressure drop over the sphere (Δp_s), which can be approximated by $\Delta p_s = p_{z=R_s} - p_{z=-R_s}$ (R_s is the radius of the sphere) and 2) the pressure drop over the remainder of the tube (Δp_f). Thus,

$$\Delta p = \Delta p_s + \Delta p_f. \tag{B1}$$

As shown in Fig. 7 *b*, the origin of the cylindrical coordinates is fixed at the center of the sphere. In these coordinates the sphere stands still, while the tube moves in the positive z direction at a constant velocity U. The diameter of the sphere D_s is slightly smaller than the diameter of the tube D_p, and the distance of a point on the spherical surface to the axisymmetrical axis is denoted r_s. Because of the linearity of low Reynolds number flow, the total pressure drop equals the sum of the pressure drop of a pure Poiseuille flow in the tube and the additional pressure drop caused by

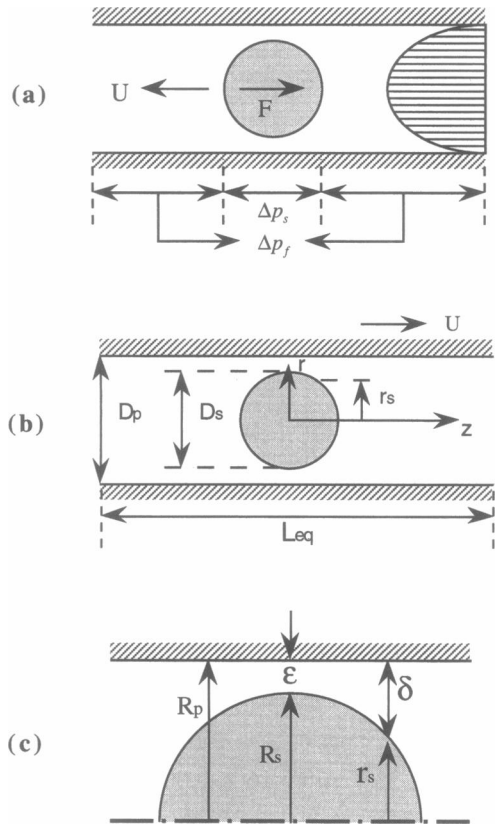

FIGURE 7 Schematic representation of the model system: (*a*) the retarded motion of a sphere at a velocity U and subjected to a force F in a circular uniform tube; (*b*) the low Reynolds number flow from the view point of the sphere, where D_p is the diameter of the tube, D_s is the diameter of the sphere, r_s is the distance of a point on the spherical surface to the axisymmetrical axis, and L_{eq} is the length of the tube; (*c*) diagram to show the definitions of R_p, R_s, r_s, ϵ, and δ.

addition of a sphere in the flow (Hochmuth and Sutera, 1970; Bungay and Brenner, 1973). Hence Δp_s is essentially the sum of this additional pressure drop and the pressure drop of a pure Poiseuille flow over a tube length of D_s, whereas Δp_f is the pressure drop of a simple Poiseuille flow over a tube length of $L_{eq} - D_s$, where L_{eq} is the total length of the tube.

First, the Navier–Stokes equations will be solved for Δp_s. For axisymmetric flow at low Reynolds number, the Navier–Stokes equations in cylindrical coordinates become (Bird et al., 1960)

$$\frac{1}{r}\frac{\partial}{\partial r}(ru) + \frac{\partial w}{\partial z} = 0, \tag{B2a}$$

$$\frac{\partial p}{\partial r} = \mu\left(\frac{\partial^2 u}{\partial r^2} + \frac{1}{r}\frac{\partial u}{\partial r} - \frac{u}{r^2} + \frac{\partial^2 u}{\partial z^2}\right), \tag{B2b}$$

$$\frac{\partial p}{\partial z} = \mu\left(\frac{\partial^2 w}{\partial r^2} + \frac{1}{r}\frac{\partial w}{\partial r} + \frac{\partial^2 w}{\partial z^2}\right), \tag{B2c}$$

where p, u, and w are the pressure, the velocity in the r direction, and the velocity in the z direction, respectively, and μ is the viscosity of the fluid.

Let $\epsilon = R_p - R_s$ (R_p is the radius of the tube) and $\delta = R_p - r_s$ (note that $r_s = R_s$ and $\delta = \epsilon$ at $z = 0$, as shown in Fig. 7 *c*). Define the dimensionless parameters $\bar{\epsilon} = (R_p - R_s)/R_p$ and $\bar{\delta} = (R_p - r_s)/R_p$. If $\bar{\epsilon}$ is small, for a small region near $z = 0$ an order-of-magnitude analysis (similar to that in boundary-layer theory) gives

$$\frac{u}{w} \approx O(\bar{\epsilon}),$$

$$\frac{(\Delta p)_r}{(\Delta p)_z} \approx O(\bar{\epsilon}^2).$$

So the Navier–Stokes equations can be further simplified as (Hochmuth and Sutera, 1970)

$$\int_{r_s}^{R_p} w \cdot 2\pi r dr = Q = \text{constant}, \tag{B3a}$$

$$\frac{dp}{dz} = \mu\left(\frac{\partial^2 w}{\partial r^2} + \frac{1}{r}\frac{\partial w}{\partial r}\right). \tag{B3b}$$

The boundary conditions are

$$w(r, z) = U \quad \text{at} \quad r = R_p, \tag{B4a}$$

$$w(r, z) = 0 \quad \text{at} \quad r = r_s(z). \tag{B4b}$$

Solving Eq. B3b and applying boundary conditions B4a and B4b yield

$$w = \frac{1}{4\mu}\frac{dp}{dz}(r^2 - r_s^2) + \left[U - \frac{1}{4\mu}\frac{dp}{dz}(R_p^2 - r_s^2)\right]\frac{\ln(r/r_s)}{\ln(R_p/r_s)}. \tag{B5}$$

The substitution of Eq. B5 into Eq. B3a gives

$$\frac{Q}{\pi}\ln\frac{r_s}{R_p} = -\frac{1}{8\mu}\frac{dp}{dz}(R_p^2 - r_s^2)\left[(R_p^2 + r_s^2)\ln\frac{r_s}{R_p} + (R_p^2 - r_s^2)\right] + \frac{U}{2}\left[2R_p^2\ln\frac{r_s}{R_p} + (R_p^2 - r_s^2)\right]. \tag{B6}$$

The definition of $\bar{\delta}$ leads to $r_s = R_p(1 - \bar{\delta})$ and $\ln(r_s/R_p) = \ln(1 - \bar{\delta})$. Consequently, $\ln(1 - \bar{\delta})$ can be expanded into Taylor series in terms of $\bar{\delta}$, and dp/dz can be solved from Eq. B6:

$$\frac{dp}{dz} = -\frac{6\mu Q}{\pi R_p^4}\left[\frac{1}{\bar{\delta}^3}\left(1 + \frac{1}{2}\bar{\delta} + \frac{7}{30}\bar{\delta}^2 + \frac{1}{10}\bar{\delta}^3 + O(\bar{\delta}^4)\right)\right] + \frac{6\mu U}{R_p^2}\left[\frac{1}{\bar{\delta}^2}\left(1 + \frac{1}{3}\bar{\delta} + \frac{3}{20}\bar{\delta}^2 + \frac{1}{15}\bar{\delta}^3 + O(\bar{\delta}^4)\right)\right]. \tag{B7}$$

For the surface of the sphere

$$\bar{\delta} = 1 - [(1 - \bar{\epsilon})^2 - \bar{z}^2]^{1/2}, \tag{B8}$$

where $\bar{z} = z/R_p$. Because $|\bar{z}| \ll 1$ in the region considered (a small region near $z = 0$),

$$\bar{\delta} \approx \bar{\epsilon} + \frac{\bar{z}^2}{2(1 - \bar{\epsilon})}, \tag{B9}$$

i.e.,

$$\bar{z} \approx [2(1 - \bar{\epsilon})(\bar{\delta} - \bar{\epsilon})]^{1/2}. \tag{B10}$$

Although all the equations derived above are for the region where $|\bar{z}| \ll 1$, they can also be applied to the region where $|\bar{z}| \ll 1$ is not strictly satisfied, because the major pressure drop occurs when $|\bar{z}| \ll 1$. Therefore, Eq. B7 can be integrated from $\bar{z} = 0$ to $\bar{z} = 1 - \bar{\delta}$, and an accurate approximation

for the pressure drop over the entire sphere will be obtained (Hochmuth and Sutera, 1970; Bungay and Brenner, 1973):

$$\Delta p_s = \frac{6\sqrt{2}\mu(1-\bar{\epsilon})^{1/2}}{R_p}\left[-\frac{Q}{\pi R_p^2}\left(J_3+\frac{1}{2}J_2+\frac{7}{30}J_1+\frac{1}{10}J_0+\cdots\right)+U\left(J_2+\frac{1}{3}J_1+\frac{3}{20}J_0+\cdots\right)\right], \tag{B11}$$

where

$$J_0 = \int_{\bar{\epsilon}}^{(1+\bar{\epsilon})/2}\frac{d\bar{\delta}}{(\bar{\delta}-\bar{\epsilon})^{1/2}} = \left(\frac{1-\bar{\epsilon}}{2}\right)^{1/2}, \tag{B12a}$$

$$J_1 = \int_{\bar{\epsilon}}^{(1+\bar{\epsilon})/2}\frac{d\bar{\delta}}{\bar{\delta}(\bar{\delta}-\bar{\epsilon})^{1/2}} = \frac{2}{\bar{\epsilon}^{1/2}}\arctan\left(\frac{1-\bar{\epsilon}}{2\bar{\epsilon}}\right)^{1/2}, \tag{B12b}$$

$$J_2 = \int_{\bar{\epsilon}}^{(1+\bar{\epsilon})/2}\frac{d\bar{\delta}}{\bar{\delta}^2(\bar{\delta}-\bar{\epsilon})^{1/2}} = \frac{\sqrt{2}(1-\bar{\epsilon})^{1/2}}{\bar{\epsilon}(1+\bar{\epsilon})} + \frac{1}{\bar{\epsilon}^{3/2}}\arctan\left(\frac{1-\bar{\epsilon}}{2\bar{\epsilon}}\right)^{1/2}, \tag{B12c}$$

$$J_3 = \int_{\bar{\epsilon}}^{(1+\bar{\epsilon})/2}\frac{d\bar{\delta}}{\bar{\delta}^3(\bar{\delta}-\bar{\epsilon})^{1/2}} = \frac{\sqrt{2}(1-\bar{\epsilon})^{1/2}}{\bar{\epsilon}(1+\bar{\epsilon})^2} + \frac{3\sqrt{2}(1-\bar{\epsilon})^{1/2}}{4\bar{\epsilon}^2(1+\bar{\epsilon})} + \frac{3}{4\bar{\epsilon}^{5/2}}\arctan\left(\frac{1-\bar{\epsilon}}{2\bar{\epsilon}}\right)^{1/2}. \tag{B12d}$$

Because the sphere moves at a constant velocity, the sum of all forces acting on the sphere must be zero, and the force balance on the sphere can be expressed as

$$\pi R_p^2\Delta p_s = \pi R_p^2\int_{-R_s}^{R_s}\frac{dp}{dz}dz = F + \int_{-R_s}^{R_s}\tau_w 2\pi R_p dz, \tag{B13}$$

where

$$\tau_w = \mu\frac{\partial w}{\partial r}\bigg|_{r=R_p} = \frac{R_p}{4}\frac{dp}{dz}\left[2-\frac{R_p^2-r_s^2}{R_p^2\ln(R_p/R_s)}\right]. \tag{B14}$$

Substituting Eqs. B7 and B14 into Eq. B13 and simplifying the result by using Taylor series will give

$$\frac{Q}{\pi R_p^2}\left(J_3-\frac{1}{2}J_2-\frac{1}{10}J_1-\frac{1}{20}J_0\right) = U\left(J_2-J_1+\frac{3}{20}J_0\right) - \frac{F}{6\sqrt{2}\pi\mu R_p(1-\bar{\epsilon})^{1/2}}. \tag{B15}$$

The substitution of Eq. B15 into Eq. B11 yields

$$\Delta p_s = \frac{\mu U}{R_p}\left[\frac{4\sqrt{2}\pi}{\bar{\epsilon}^{1/2}}-\frac{71}{5}+O(\bar{\epsilon}^{1/2})\right] + \frac{F}{\pi R_p^2}\left[1+\frac{4}{3}\bar{\epsilon}+\frac{16}{9}\bar{\epsilon}^2+O(\bar{\epsilon}^{5/2})\right]. \tag{B16}$$

Equation (B16) clearly shows how the existence of F slows the motion of the sphere.

The second term in Eq. B1, Δp_f, can be estimated from the mean velocity of the fluid relative to the tube, which can be solved from Eq. B15 as

$$V_m = \frac{Q}{\pi R_p^2} - U = -U\left[1-\frac{4}{3}\bar{\epsilon}+\frac{16^2}{9}+O(\bar{\epsilon}^{5/2})\right] - \frac{F}{\pi\mu R_p}\left[\frac{2\sqrt{2}}{9\pi}\bar{\epsilon}^{5/2}-\frac{8}{9\pi^2}\bar{\epsilon}^3+O(\bar{\epsilon}^{7/2})\right]. \tag{B17}$$

Thus Δp_f can readily be calculated as

$$\Delta p_f = -\frac{8\mu(L_{eq}-D_s)}{R_p^2}V_m = \frac{8\mu(L_{eq}-D_s)U}{R_p^2}\left[1-\frac{4}{3}\bar{\epsilon}+\frac{16}{9}\bar{\epsilon}^2+O(\bar{\epsilon}^{5/2})\right] + \frac{8(L_{eq}-D_s)F}{\pi R_p^3}\left[\frac{2\sqrt{2}}{9\pi}\bar{\epsilon}^{5/2}-\frac{8}{9\pi^2}\bar{\epsilon}^3+O(\bar{\epsilon}^{7/2})\right]. \tag{B18}$$

Compared with those in Eq. B16, both terms in Eq. B18 seem to be higher-order terms. However, although $\bar{\epsilon}$ is small, L_{eq} could be so large that Δp_f is of the same order as Δp_s or even greater. Therefore, Δp_f cannot simply be ruled out of the total pressure drop. Finally, the combination of Eqs. B1, B16, and B18 gives

$$\Delta p = \frac{\mu U}{R_p}\left[\left(\frac{4\sqrt{2}\pi}{\bar{\epsilon}^{1/2}}-\frac{71}{5}\right)+\frac{8(L_{eq}-D_s)}{R_p}\left(1-\frac{4}{3}\bar{\epsilon}\right)\right] + \frac{F}{\pi R_p^2}\left[\left(1+\frac{4}{3}\bar{\epsilon}\right)+\frac{8(L_{eq}-D_s)}{R_p}\left(\frac{2\sqrt{2}}{9\pi}\bar{\epsilon}^{5/2}-\frac{8}{9\pi^2}\bar{\epsilon}^3\right)\right]. \tag{B19}$$

Now the relationship among Δp, F, and U are discussed for two special cases: $U = 0$ and $F = 0$.

For a stationary sphere ($U = 0$), the pressure drop over the sphere and the force on it can be solved from Eqs. B11 and B15:

$$\pi R_p^2\Delta p_s = -\frac{9\sqrt{2}\pi\mu Q}{4R_p\bar{\epsilon}^{5/2}}\left[1+\frac{2\sqrt{2}}{\pi}\bar{\epsilon}^{1/2}+\frac{1}{6}\bar{\epsilon}+\frac{59}{360}\bar{\epsilon}^2+O(\bar{\epsilon}^{5/2})\right], \tag{B20a}$$

$$F = -\frac{9\sqrt{2}\pi\mu Q}{4R_p\bar{\epsilon}^{5/2}}\left[1+\frac{2\sqrt{2}}{\pi}\bar{\epsilon}^{1/2}-\frac{8\sqrt{2}}{3\pi}\bar{\epsilon}^{3/2}-\frac{7}{120}\bar{\epsilon}^2+O(\bar{\epsilon}^{5/2})\right]. \tag{B20b}$$

From the definition of $\bar{\epsilon} = (R_p - R_s)/R_s$, Bungay and Brenner (1973) solved this problem by using singular perturbation techniques. Although their explicit expressions for $\pi R_p^2\Delta p_s$ and F are not exactly the same as in Eq. B20, the relative magnitude between these two quantities shows good

agreement with the result obtained from the lubrication theory (Fig. 8):

$$\frac{F}{\pi R_p^2 \Delta p_s} = 1 - \frac{4}{3}\bar{\epsilon} + O(\bar{\epsilon}^{5/2})$$

(lubrication theory), (B21a)

$$\frac{F}{\pi R_p^2 \Delta p_s} = 1 - \frac{4}{3}\bar{\epsilon} + \frac{58}{45}\bar{\epsilon}^2 + O(\bar{\epsilon}^3)$$

(Bungay and Brenner, 1973). (B21b)

After the incorporation of the fluid flow effect, the force on a stationary sphere can be expressed as

$$F = \frac{\pi R_p^2 \Delta p}{\left(1 + \frac{4}{3}\bar{\epsilon}\right) + \frac{8(L_{eq} - D_s)}{R_p}\left(\frac{2\sqrt{2}}{9\pi}\bar{\epsilon}^{5/2} - \frac{8}{9\pi^2}\bar{\epsilon}^3\right)}. \quad \text{(B22)}$$

For a neutrally buoyant sphere ($F = 0$), Eq. B16 can be simplified as

$$\frac{\Delta p_s}{\mu U / R_p} = \frac{4\sqrt{2}\pi}{\bar{\epsilon}^{1/2}} - \frac{71}{5} + O(\bar{\epsilon}^{1/2}), \quad \text{(B23)}$$

which is consistent with previous results (Hochmuth and Sutera, 1970; Bungay and Brenner, 1973). The total pressure drop and the velocity of the sphere are related by (Eq. B19)

$$\Delta p = \frac{\mu U}{R_p}\left[\left(\frac{4\sqrt{2}\pi}{\bar{\epsilon}^{1/2}} - \frac{71}{5}\right) + \frac{8(L_{eq} - D_s)}{R_p}\left(1 - \frac{4}{3}\bar{\epsilon}\right)\right]. \quad \text{(B24)}$$

APPENDIX C. APPARENT FILM THICKNESS, ϵ

In Eq. B24, all quantities are measurable or known except L_{eq} and $\bar{\epsilon}$ (note that $D_s = D_p(1 - \bar{\epsilon})$). Because we have determined L_{eq} by measuring the velocities of small particles (Appendix A), we can calculate $\bar{\epsilon}$ from Eq. B24 by measuring the velocities of drag-free spherical neutrophils. In reality, a neutrophil has many microvilli projecting from its surface. So the gap between a neutrophil surface and a micropipette wall is not so ideal as drawn in Fig. 7, and therefore the magnitude of this gap will be called "the apparent film thickness," which is still represented by ϵ. Fig. 3 shows the velocities of two neutrophils in a 9.5-μm pipette under different suction pressures. From the slope of the line, $\bar{\epsilon}$ was solved to be 0.024, corresponding to a gap width of 0.1 μm. If all the velocities of unattached neutrophils in the tether-formation experiments are plotted, they all fall around the fitted line, and only a slightly smaller value for $\bar{\epsilon}$ will be obtained if the fitted line for all the data is used.

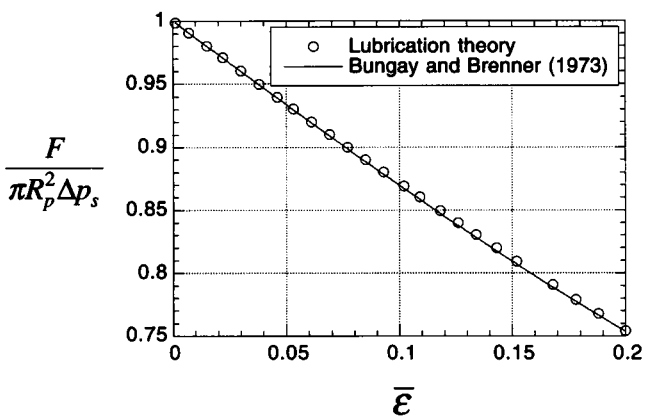

FIGURE 8 Comparison of the lubrication theory solution (Eq. B21a) and the solution by Bungay and Brenner (1973) (Eq. B21b).

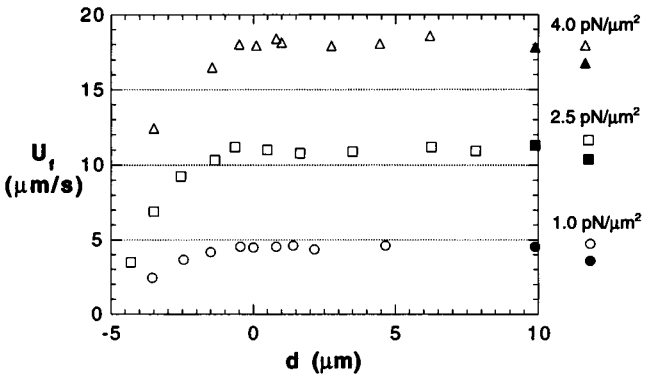

FIGURE 9 Velocities (U_f) of a neutrophil at different suction pressures when the bead pipette was positioned at different distances d, where d is the distance from the opening of the pipette holding the neutrophil and the proximal edge of the bead, e.g., when $d = 0$ the edge of the bead just touches the diametral plane at the opening of the pipette. ▲, ■, ●, results when the bead pipette was removed completely from the field of view.

In our experimental system a bead held by a micropipette exists at the opening of the neutrophil pipette. To determine whether the position of this bead has a major effect on the flow of neutrophils inside the pipette, we measured the velocities of neutrophils inside the micropipette by positioning the bead at different distances from the opening of the neutrophil pipette in the pressure range that was used in the tether-formation experiments. As shown in Fig. 9, the bead would not affect the flow of neutrophils much if the bead were positioned outside the neutrophil pipette opening.

APPENDIX D. CALCULATION OF FORCE

If a neutrophil is stationary after adhesion to a bead, the force on the neutrophil, F, can be calculated from Eq. B22. Essentially, by use of the equivalent length of the micropipette (Appendix A) and the apparent film thickness (Appendix C), an order-of-magnitude analysis can be performed for the denominator of Eq. B22:

$$\frac{8(L_{eq} - D_s)}{R_p}\left(\frac{2\sqrt{2}}{9\pi}\bar{\epsilon}^{5/2} - \frac{8}{9\pi^2}\bar{\epsilon}^3\right) \approx 0.8\%,$$

$$\frac{4}{3}\bar{\epsilon} \approx 3.2\%.$$

Therefore one can directly employ Eq. 1 to calculate the force exerted on a stationary neutrophil with an error below 5%.

If the neutrophil is still moving after the adhesion to the bead (implying that a membrane tether has formed between the neutrophil and the bead, as shown in Fig. 4 *b*), the force on the neutrophil will not be so large as the value calculated from Eq. 1. In fact, the relationship among Δp, F (the force on the neutrophil), and U_t (the velocity of the tethered neutrophil) can be expressed by Eq. B19 (higher-order terms have been neglected):

$$\Delta p = \frac{\mu U_t}{R_p}\Phi\left(\bar{\epsilon}, \frac{L_{eq}}{R_p}\right) + \frac{F}{\pi R_p^2}, \quad \text{(D1)}$$

where Φ stands for a function. When the same neutrophil moves freely in the same pipette ($F = 0$) under the same pressure, it will move at a different

velocity U_f, which is related to Δp as

$$\Delta p = \frac{\mu U_f}{R_p} \Phi\left(\bar{\epsilon}, \frac{L_{eq}}{R_p}\right). \quad \text{(D2)}$$

From Eqs. D1 and D2, F can be readily solved as

$$F = \pi R_p^2 \Delta p \left[1 - \frac{U_t}{U_f}\right]. \quad \text{(D3)}$$

REFERENCES

Alon, R., D. A. Hammer, and T. A. Springer. 1995. Lifetime of the P-selectin-carbohydrate bond and its response to tensile force in hydrodynamic flow. *Nature (London).* 374:539–542.

Ashkin, A. 1992. Forces of a single-beam gradient laser trap on a dielectric sphere in the ray optics regime. *Biophys. J.* 61:569–582.

Binnig, G., C. F. Quate, and C. Gerber. 1986. Atomic force microscope. *Phys. Rev. Lett.* 56:930–933.

Bird, R. B., W. E. Stewart, and E. N. Lightfoot. 1960. Transport Phenomena. John Wiley & Sons, Inc., New York.

Bungay, P. M., and H. Brenner. 1973. The motion of a closely-fitting sphere in a fluid-filled tube. *Int. J. Multiphase Flow.* 1:25–56.

Dai, J., and M. P. Sheetz. 1995. Mechanical properties of neuronal growth cone membrane studied by tether formation with laser optical tweezers. *Biophys. J.* 68:988–996.

Dammer, U., O. Popescu, P. Wagner, D. Anselmetti, H.-J. Guntherodt, and G. N. Misevic. 1995. Binding strength between cell adhesion proteoglycans measured by atomic force microscopy. *Science.* 267:1173–1175.

Dembo, M., D. C. Torney, K. Saxman, and D. Hammer. 1988. The reaction-limited kinetics of membrane-to-surface adhesion and detachment. *Proc. R. Soc. London Ser. B* 234:55–83.

Erlandsen, S. L., S. R. Hasslen, and R. D. Nelson. 1993. Detection and spatial distribution of the β_2 integrin (Mac-1) and L-selectin (LECAM-1) adherence receptors on human neutrophils by high-resolution field emission SEM. *J. Histochem. Cytochem.* 41:327–333.

Evans, E. A. 1973. New membrane concept applied to the analysis of fluid shear- and micropipette-deformed red blood cells. *Biophys. J.* 13: 941–953.

Evans, E., D. Berk, and A. Leung. 1991. Detachment of agglutinin-bonded red blood cells: I. Forces to rupture molecular-point attachments. *Biophys. J.* 59:838–848.

Evans, E., and B. Kukan. 1984. Passive material behavior of granulocytes based on large deformation and recovery after deformation tests. *Blood.* 64:1028–1035.

Evans, E., K. Ritchie, and R. Merkel. 1995. Sensitive force technique to probe molecular adhesion and structural linkages at biological interfaces. *Biophys. J.* 68:2580–2587.

Evans, E., and A. Yeung. 1989. Apparent viscosity and cortical tension of blood granulocytes determined by micropipette aspiration. *Biophys. J.* 56:151–160.

Finer, J. T., R. M. Simmons, and J. A. Spudich. 1994. Single myosin molecule mechanics: piconewton forces and nanometer steps. *Nature (London).* 368:113–119.

Florin, E.-L., V. T. Moy, and H. E. Gaub. 1994. Adhesion forces between individual ligand-receptor pairs. *Science.* 264:415–417.

Happel, J., and H. Brenner. 1983. Low Reynolds Number Hydrodynamics. Martinus Nijhoff Publishers, Dordrecht, The Netherlands.

Hochmuth, R. M., E. A. Evans, H. C. Wiles, and J. T. McCown. 1983. Mechanical measurement of red cell membrane thickness. *Science.* 220:101–102.

Hochmuth, R. M., J.-Y. Shao, J. Dai, and M. P. Sheetz. 1996. Deformation and flow of membrane into tethers extracted from neuronal growth cones. *Biophys. J.* 70:358–369.

Hochmuth, R. M., and S. P. Sutera. 1970. Spherical caps in low Reynolds-number tube flow. *Chem. Eng. Sci.* 25:593–604.

Hoh, J. H., J. P. Cleveland, C. B. Prater, J.-P. Revel, and P. K. Hansma. 1992. Quantized adhesion detected with the atomic force microscope. *J. Am. Chem. Soc.* 114:4917–4918.

Ishijima, A., T. Doi, K. Sakurada, and T. Yanagida. 1991. Sub-piconewton force fluctuations of actomyosin in vitro. *Nature (London).* 352: 301–306.

Kamimura, S., and K. Takahashi. 1981. Direct measurement of the force of microtubule sliding in flagella. *Nature (London).* 293:566–568.

Kishino, A., and T. Yanagida. 1988. Force measurements by micromanipulation of a single actin filament by glass needles. *Nature (London).* 334:74–76.

Kojima, H., A. Ishijima, and T. Yanagida. 1994. Direct measurement of stiffness of single actin filaments with and without tropomyosin by in vitro nanomanipulation. *Proc. Natl. Acad. Sci. USA.* 91:12962–6.

Kuo, S. C., and M. Sheetz. 1992. Optical tweezers in cell biology. *Trends Cell Biol.* 2:116–118.

Kuo, S. C., and M. Sheetz. 1993. Force of single kinesin molecules measured with optical tweezers. *Science.* 260:232–234.

Mitchison, J. M., and M. M. Swann. 1954. The mechanical properties of the cell surface: I. The cell elastimeter. *J. Exp. Biol.* 31:443–460.

Moy, V. T., E.-L. Florin, and H. E. Gaub. 1994. Intermolecular forces and energies between ligands and receptors. *Science.* 266:257–259.

Needham, D., M. Armstrong, D. L. Hatchell, and R. S. Nunn. 1989. Rapid deformation of "passive" polymorphonuclear leukocytes: the effects of pentoxifylline. *J. Cell. Physiol.* 140:549–557.

Needham, D., and R. M. Hochmuth. 1992. A sensitive measure of surface stress in the resting neutrophil. *Biophys. J.* 61:1664–1670.

Picker, L. J., R. A. Warnock, A. R. Burns, C. M. Doerschuk, E. L. Berg, and E. C. Butcher. 1991. The neutrophil selectin LECAM-1 presents carbohydrate ligands to the vascular selectins ELAM-1 and GMP-140. *Cell.* 66:921–933.

Rand, R. P., and A. C. Burton. 1964. Mechanical properties of the red cell membrane. *Biophys. J.* 4:115–135.

Waugh, R. E., and R. G. Bauserman. 1995. Physical measurements of bilayer-skeletal separation forces. *Ann. Biomed. Eng.* 23:308–321.

Waugh, R. E., and R. M. Hochmuth. 1987. Mechanical equilibrium of thick, hollow, liquid membrane cylinders. *Biophys. J.* 52:391–400.

Zhelev, D. V., and D. Needham. 1993. Tension-stabilized pores in giant vesicles: determination of pore size and pore line tension. *Biochim. Biophys. Acta.* 1147:89–104.

Zhelev, D. V., D. Needham, and R. M. Hochmuth. 1994. Role of the membrane cortex in neutrophil deformation in small pipets. *Biophys. J.* 67:696–705.